ADVANCED QUANTUM TECHNOLOGIES
www.advquantumtech.com

Ion Transport and Reordering in a 2D Trap Array

Yong Wan, Robert Jördens, Stephen D. Erickson, Jenny J. Wu, Ryan Bowler, Ting Rei Tan, Pan-Yu Hou, David J. Wineland,* Andrew C. Wilson, and Dietrich Leibfried*

Scaling quantum information processors is a challenging task, requiring manipulation of a large number of qubits with high fidelity and a high degree of connectivity. For trapped ions, this can be realized in a 2D array of interconnected traps in which ions are separated, transported, and recombined to carry out quantum operations on small subsets of ions. Here, functionality of a junction connecting orthogonal linear segments in a 2D trap array to reorder a two-ion crystal is demonstrated. The secular motion of the ions experiences low energy gain and the internal qubit levels maintain coherence during the reordering process, therefore demonstrating a promising method for providing all-to-all connectivity in a large-scale, 2D or 3D trapped-ion quantum information processor.

1. Introduction

Coherent manipulation of trapped atomic ions enables applications ranging from quantum sensing (e.g., force and field sensing, precision spectroscopy, optical clocks) to quantum information processing. Most applications must deal with the difficulty in controlling multiple ions. For optical clocks the number of clock ions limits the ultimate frequency stability,[1] and for quantum information processing the number of qubits limits the processing capability. All quantum computing platforms[2] can be scaled up by modularization. In ion traps, this can be done by confining individual ions or small groups of ions in separate trap zones of an array. Ions are then connected either through probabilistic ion–photon coupling,[3,4] or as discussed here, by employing the "quantum charge-coupled device" (QCCD) architecture,[5,6] in which ions are transported throughout the array to provide the high connectivity required for efficient implementation of general algorithms. This approach can extend the processes performed routinely with small ion crystals, such as high-fidelity quantum gates[7,8] and precise preparation and characterization of the motional state,[9] to a larger number of qubits, while maintaining low cross-talk during quantum gates and state readout.[10]

One of the key elements of the QCCD architecture is the ability to reconfigure ion crystals and to hold subsets of ions in different locations, ensuring mutual isolation, while operating on them in parallel. High connectivity and parallelism are considered crucial for large-scale fault-tolerant quantum computation.[11] This requires separation, transport, and rearrangement of ions throughout multiple trapping zones. Previous experiments have demonstrated adiabatic transport of both single ions[12] and chains of ions,[13] diabatic transport and separation,[14,15] and fast swapping of neighboring ions in a 1D array by rotating two ions in place.[16–18] These primitives have enabled a transport-based quantum logic gate,[19,20] scalable creation of multi-partite entanglement with bipartite interactions,[21] quantum-state-assisted sensing,[22] tests of local realism,[23] and quantum gate teleportation.[24] Since high-fidelity multi-qubit gates require the motion to be near its ground state, transport primitives with low motional excitation would be highly beneficial to all of these applications.

Specific to developing a trapped-ion quantum computer, a multi-dimensional trap array is desired to fully realize the potential of the QCCD architecture, in which multiple linear trap segments are connected by junctions.[12,13,25–29] Such a multi-dimensional trap array enables smaller average distances between ions than in lower-dimensional architectures and efficiently extends the all-to-all coupling between ions in a small chain[30] to connecting arbitrary subsets of a larger number of qubits.

Dr. Y. Wan, Dr. R. Jördens, S. D. Erickson, J. J. Wu, Dr. R. Bowler, Dr. T. R. Tan, Dr. P.-Y. Hou, Prof. D. J. Wineland, Dr. A. C. Wilson, Dr. D. Leibfried
National Institute of Standards and Technology
Boulder, CO 80305, USA
E-mail: wanyong@nim.ac.cn; djw34@uoregon.edu
Dr. Y. Wan, Dr. R. Jördens, S. D. Erickson, J. J. Wu, Dr. R. Bowler, Dr. T. R. Tan, Dr. P.-Y. Hou, Prof. D. J. Wineland
Department of Physics
University of Colorado
Boulder, CO 80309, USA
Dr. Y. Wan
National Institute of Metrology
18 Changchi Road, Changping District, Beijing 102200, China
Dr. R. Jördens
QUARTIQ GmbH
Berlin, Germany
Dr. R. Bowler
EOSpace Inc.
6222 185th Avenue Northeast, Redmond, WA 98052, USA
Dr. T. R. Tan
ARC Centre for Engineered Quantum Systems
School of Physics
The University of Sydney
Sydney, NSW 2006, Australia
Prof. D. J. Wineland
Department of Physics
University of Oregon
Eugene, OR 97403, USA

DOI: 10.1002/qute.202000028

Previous work in traps featuring a junction demonstrated the low-temperature shuttling of ions through radio-frequency (RF) junctions and characterized the resulting kinetic energy increase.[12,13] Ion crystal reconfigurations were reported in refs. [25, 29] (using junctions but without measurement of kinetic energy changes) or using crystal rotation in a 1D architecture.[16–18] Recently, crystal rotations were executed in parallel in different trap zones, illustrating the potential of scaling this technique.[31] Here, we use a junction to distribute $^9Be^+$ ions in a 2D architecture and reorder two ions initially in the same potential by combining adiabatic transport and separation primitives. We show that the coherence in the internal states of the ions is maintained during the process and characterizes excess motional excitation.

2. Experimental Section

A schematic of the trap array is shown in **Figure 1**a.[12,32] The physical structure consisted of two electrode wafers separated by 250 µm, providing strong confinement along all three directions, and a third layer (500 µm below the bottom layer) possessing one single electrode that served as a common bias electrode across the entire trap. The trap featured three linear regions along the $-z$, $+z$, and $+x$ directions (containing zones *S*, *H*, and *V*, respectively) with the origin located at the center of the RF junction (*C*) in a plane that was parallel to, and in the middle between the two electrode wafers. All other relevant zones (*L*, *A*, *B*, *R*) for this work are marked in **Figure 2**. The X-shaped junction (X-junction) at *C* allowed us to route ions to *S*, *H*, and *V*. Deviation from an ideal infinitely long linear Paul trap gave rise to pseudo-potential "bumps" around *C* along the *x*- and *z*-directions as illustrated in Figure 1b. Besides complicating ion transport, this had further implications for quantum information experiments, such as a position-dependent RF modulation index[33] which affected laser-based operations and position-dependent qubit frequencies from trap-RF-induced AC-Zeeman shifts. These pseudo-potential bumps also introduced additional motional heating originating from noise in the RF gradients.[12] More details on the trap can be found in refs. [12, 13, 32]. All laser beams for coherent manipulation, state preparation, and state detection were focused to zone *S* with waists of ≈ 25 µm, while ions in nearby trapping zones were at least 390 µm away during illumination of ions in *S*. Qubits in first-order magnetic-field-insensitive hyperfine ground states of $^9Be^+$ ions, with $|F=1, m_F=1\rangle \equiv |\uparrow\rangle$ and $|2,0\rangle \equiv |\downarrow\rangle$ were encoded.[34] Prior to state detection, $|\uparrow\rangle$ was transferred to $|2,2\rangle \equiv |\text{Bright}\rangle$ and $|\downarrow\rangle$ to $|1,-1\rangle \equiv |\text{Dark}\rangle$. A resonant laser driving the $S_{1/2}\,|2,2\rangle \leftrightarrow P_{3/2}\,|3,3\rangle$ cycling transition was used to distinguish the two states through fluorescence photon counts.[35–37] The motional heating and excess energy accumulated during certain transport primitives were investigated by running the test sequences listed in **Table 1**. High motional excitation after transport reduced the fidelity of subsequent quantum gates or required additional time to be spent on sympathetic cooling. To characterize a primitive, a single $^9Be^+$ ion or two $^9Be^+$ ions were initialized in *S* by laser cooling the axial modes ($\omega_{COM} = 2\pi \times 3.6$ MHz, $\omega_{STR} = 2\pi \times 6.2$ MHz) of the ions close to the motional ground state ($\bar{n} = 0.016(2)$ for a single ion, $\bar{n}_{COM} = 0.038(9)$ and $\bar{n}_{STR} = 0.014(7)$ for two ions). The radial modes (mode frequencies 11 – 13 MHz) were left close to the Doppler temperature corresponding to an average motional occupation number $\bar{n}$ of ≈ 0.5. After completing a transport test sequence and returning to *S*, the final state of the ion motion was probed with motion-sensitive Raman transition beams tuned to blue and red sidebands[38,39] in separate experiments. Assuming a thermal distribution of final energies, $\bar{n}$ of the ion motional modes were extracted by fitting a Rabi-oscillation model to the data from both experiments. More details of the motional-state analysis are provided in the Supporting Information.

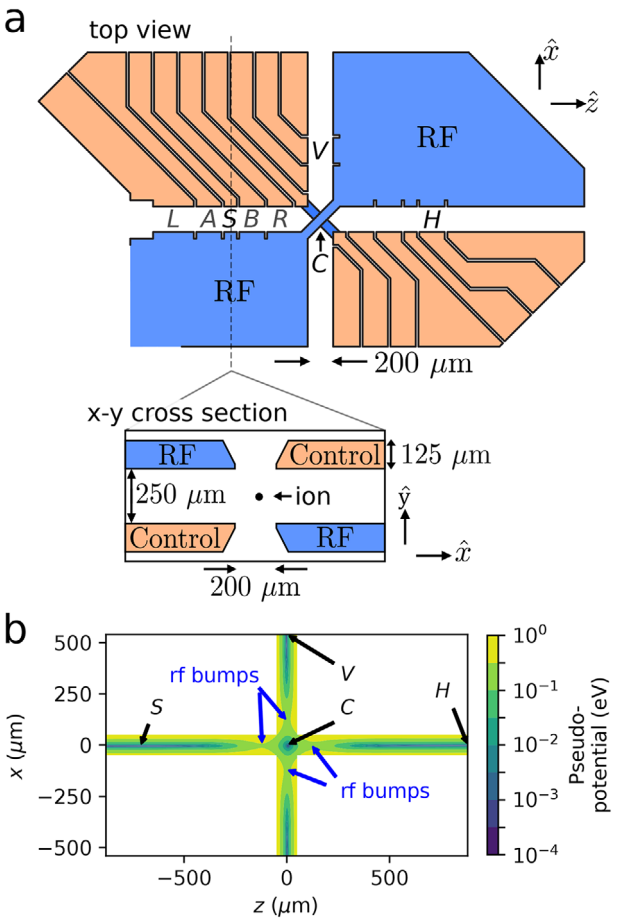

Figure 1. Schematic of the X-junction trap. a) Schematic view of the top wafer of the trap, with DC (control) electrodes in orange and RF electrodes in blue. A second wafer below the top wafer has DC and RF electrodes swapped, as indicated in the cross-section. The ion shown is located on the axis $x = y = 0$ of a linear portion of the trap. The ions are held in three major experiment zones, labeled by *S*, *H*, and *V*, connected by the junction located at *C*. Trapping zones *L*, *A*, *B*, and *R* lying in the same linear region as *S* are used together with the zone *S* to perform operations such as separation, recombination, and individual addressing and detection. (See text for more details.) b) Pseudo-potential along the linear channels connected by the junction in the plane equidistant to the two wafers defined to be $y = 0$. The junction gives rise to four pseudo-potential bumps (positions indicated by blue arrows) around *C*.

Several of the experimentally implemented transport primitives are now described in more detail (see also Table 1 for a summary). Two $^9Be^+$ ions (*a* and *b*) were trapped in a single well *S* and subsequently separated them from an initial spacing of ≈ 5 µm into two individual wells located at *A* and *B*. The well minima

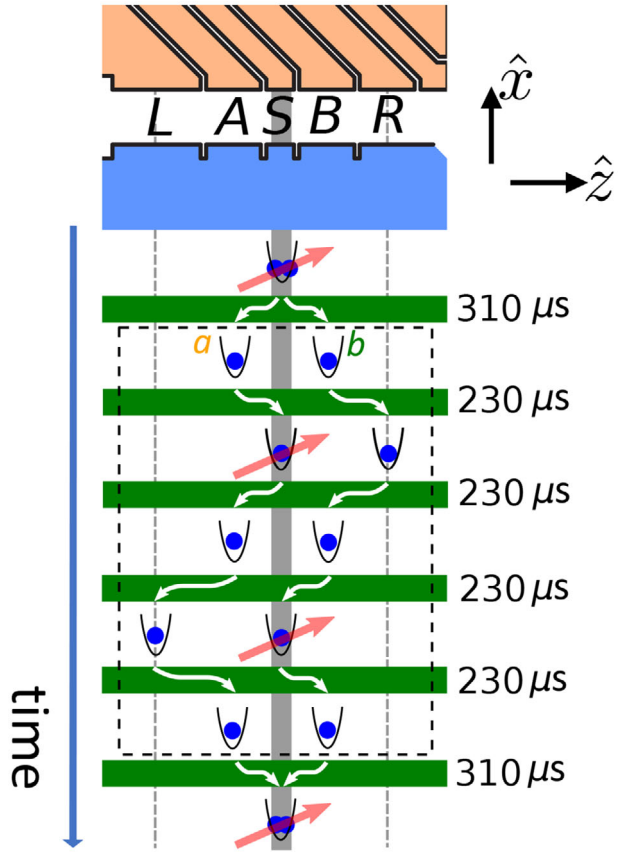

Figure 2. Individual addressing and detection sequence. Using the sequence depicted within the dashed lines, ions in each well can be manipulated and detected individually, with the shuttling operations in the dashed box taking ≈ 1 ms. Ions *a* and *b* are first separated into zones *A* and *B*, and then *a* is shuttled into *S* while *b* moves to zone *R*. This formation allows for internal state manipulation and detection of *a*. When *a* is shifted to *L*, ion *b* enters *S* and can be manipulated and/or its state detected.

were separated by ≈ 340 μm and are formed in ≈ 310 μs by ramping the harmonic and quartic terms of the potential.[40] A suitable static electric field along the axial direction of the crystal, superimposed on the separation waveform, shifted the center of the ion crystal relative to the center of the quartic potential, enabling control over the number of ions transported into the respective individual wells.[14] When separating two ions into wells *A* and *B*, this primitive was denoted as $S_{ab} \rightarrow A_a B_b$ in Table 1 (row 6). Here, the symbols before and after the right arrow denoted the initial and final configurations of the primitive, respectively. The capital letters of a configuration denoted the positions of the wells, and the subscripts denoted the ion(s) residing in each well, respectively. Each ion traveled a distance of ≈ 167.5 μm. To characterize $S_{ab} \rightarrow A_a B_b$, a longer test sequence $S_{ab} \rightarrow A_a B_b \rightarrow S_{ab}$ was run, which was implemented by concatenating the forward and reversed version of the primitive $S_{ab} \rightarrow A_a B_b$, and measured the excitation in the center-of-mass (COM) and stretch (STR) mode after recombination of *a* and *b* in *S* (the well in which the motional state was characterized at the end of a test sequence is underlined in Table 1). An average COM mode occupation of $\bar{n}$=0.55(3) and 0.43(3) in the STR mode was found.

An important shuttling sequence, illustrated in the dashed box in Figure 2, was referred to as the "individual addressing and detection sequence'

$$A_i B_j \rightarrow S_i R_j \rightarrow A_i B_j \rightarrow L_i S_j \rightarrow A_i B_j \tag{1}$$

Additional laser pulses were applied during configurations $S_i R_j$ and $L_i S_j$ to manipulate the ions' internal states individually after separation and before detection (Figure 2). This allowed to individually rotate each ion on its qubit Bloch sphere. The total duration of the transport in the individual addressing and detection sequence, not including any manipulation or detection operations, was ≈ 1 ms. This sequence can also be used to determine the number of ions in each well.

Combining $S_{ab} \rightarrow A_a B_b$ with the individual addressing and detection sequence allowed to probe the temperature of individual ions. To this end, motion-sensitive Raman beams were applied in the configuration $S_a R_b$ to determine the temperature of the ion *a* in the left well, and $L_a S_b$ for the ion *b* in the right well, deriving average occupation numbers of 0.10(1) and 0.25(2), respectively, using sideband thermometry.[38]

The speed of the transport primitives in Table 1 is limited by low-pass filters that serve to reduce electric field noise on the trap electrodes.[32] While low field noise was essential to achieve high-fidelity gates, the filters were not compatible with fast transport. Therefore, future experiments would benefit from fast switching between a "transport configuration" and a "gate configuration." The transport primitives investigated here all give an energy gain of less than one quantum. From this, the infidelity of a phase or Mølmer and Sørensen gate caused by a thermally occupied gate mode can be estimated by $\epsilon_{\bar{n}} = \frac{\pi^2 \eta^4}{4} \bar{n}(2\bar{n}+1)$, which yielded an error of 0.01 for $\bar{n} = 1$ and Lamb–Dicke parameter $\eta = 0.19$. This error was too large for fault-tolerant quantum computing and was avoided by applying sympathetic cooling immediately after transport. The length of this cooling was decreased if transport was performed with low energy gain.

3. Reordering Two Ions

By combining further transport primitives (see Table 1 for their individual characteristics), we demonstrate reordering of a two-ion crystal by separating ions *a* and *b* and then moving the ions around each other with the aid of the X-junction. This is done by separating a two-ion crystal $S_{ab} \rightarrow A_a B_b$, shuttling of ion *b* to *V* ($A_a B_b \rightarrow A_a C_b \rightarrow A_a V_b$, step I in **Figure 3**a), shuttling ion *a* to *H* ($A_a V_b \rightarrow C_a V_b \rightarrow H_a V_b$, step II), moving ion *b* to *A* ($H_a V_b \rightarrow H_a C_b \rightarrow H_a A_b$, step III), moving ion *a* to *B* ($H_a A_b \rightarrow C_a A_b \rightarrow B_a A_b$, step IV), and combining *a* and *b* ($B_a A_b \rightarrow S_{ba}$). The full reordering sequence reads

$$\begin{aligned} S_{ab} &\rightarrow A_a B_b \rightarrow A_a C_b \rightarrow A_a V_b \rightarrow C_a V_b \rightarrow H_a V_b \\ &\rightarrow H_a C_b \rightarrow H_a A_b \rightarrow C_a A_b \rightarrow B_a A_b \rightarrow S_{ba} \end{aligned} \tag{2}$$

with the duration of each individual segment listed in Table 1. The duration of the reordering sequence without separation and recombination ($A_a B_b$ to $B_a A_b$) is ≈ 1.1 ms.

Table 1. Summary of transport primitives for $^9Be^+$ ions.

#	Primitive	Test sequence	Crystal	$\bar{n}$	Duration (μs)	Distance (μm)	Δn_p
1	$S_a \rightarrow A_a$	$S_a \rightarrow A_a \rightarrow \underline{S_a}$	$^9Be^+$	0.045(3)	68	170	0.015(2)
2	$A_a \rightarrow C_a$	$S_a \rightarrow A_a \rightarrow C_a \rightarrow A_a \rightarrow \underline{S_a}$	$^9Be^+$	0.12(1)	128	880	0.038(5)
3	$H_a \rightarrow C_a$	$S_a \rightarrow A_a \rightarrow C_a \rightarrow H_a \rightarrow C_a \rightarrow A_a \rightarrow \underline{S_a}$	$^9Be^+$	0.27(1)	128	880	0.075(7)
4	$C_a \rightarrow C'_a$	$S_a \rightarrow A_a \rightarrow C_a \rightarrow C'_a \rightarrow C_a \rightarrow A_a \rightarrow \underline{S_a}$	$^9Be^+$	0.23(1)	57	-	0.055(7)
5	$V_a \rightarrow C_a$	$S_a \rightarrow A_a \rightarrow C_a \rightarrow C'_a \rightarrow V_a \rightarrow C'_a \rightarrow C_a \rightarrow A_a \rightarrow \underline{S_a}$	$^9Be^+$	0.30(2)	132	540	0.04(1)
6	$S_{ab} \rightarrow A_aB_b$	$S_{ab} \rightarrow A_aB_b \rightarrow \underline{S_{ab}}$	$^9Be^+$-$^9Be^+$	0.55(3) (COM) 0.43(3) (STR)	310	167.5/167.5	-
7	$A_aB_b \rightarrow S_aR_b$	$S_{ab} \rightarrow A_aB_b \rightarrow \underline{S_aR_b} \rightarrow A_aB_b \rightarrow L_aS_b \rightarrow A_aB_b \rightarrow S_{ab}$	$^9Be^+$-$^9Be^+$	0.10(1)	230	160/220	-
8	$A_aB_b \rightarrow L_aS_b$	$S_{ab} \rightarrow A_aB_b \rightarrow S_aR_b \rightarrow A_aB_b \rightarrow L_a\underline{S_b} \rightarrow A_aB_b \rightarrow S_{ab}$	$^9Be^+$-$^9Be^+$	0.25(2)	230	280/160	-
9	$A_aB_b \rightarrow A_aC_b$	$S_{ab} \rightarrow A_aB_b \rightarrow A_aC_b \rightarrow A_aB_b \rightarrow \underline{S_aR_b} \rightarrow A_aB_b \rightarrow L_aS_b \rightarrow A_aB_b \rightarrow S_{ab}$	$^9Be^+$-$^9Be^+$	0.13(1)	110	0/540	0.015(7)
10	$A_aB_b \rightarrow A_aC_b$	$S_{ab} \rightarrow A_aB_b \rightarrow A_aC_b \rightarrow A_aB_b \rightarrow S_aR_b \rightarrow A_aB_b \rightarrow L_a\underline{S_b} \rightarrow A_aB_b \rightarrow S_{ab}$	$^9Be^+$-$^9Be^+$	0.63(4)	110	0/540	0.19(2)

To characterize the performance of each primitive, a test sequence is used where the motional excitation is measured in one well configuration (underlined) toward the end or in the middle of the test sequence. At the beginning of the test sequence, the axial modes of ion crystals are cooled close to the motional ground states ($\bar{n} = 0.016(2)$ for a single ion, $\bar{n}_{COM} = 0.038(9)$ and $\bar{n}_{STR} = 0.014(7)$ for two ions). The symbols C and C' here indicate the same trapping zone, but with the weakest axis of the trapping potential aligned with the z-axis and x-axis, respectively. Subtracting the initial $\bar{n}$ after ion preparation and excitations during common sections in the test sequences allows us to derive the excess motional excitation per transport primitive Δn_p. If a primitive is run forward and backward, we assume that these two parts contribute equally to Δn_p. The test sequence for determining the motional excitation of the primitive $S_{ab} \rightarrow A_aB_b$ (row 6) includes mode mixing in the process of separation and recombination, therefore no values for Δn_p are derived. As a consequence, there is no prediction of motional excitations in the well configuration A_aB_b, and the measurement results in row 7–8 are used as the baseline for the test sequences in the rows below.

The transport waveforms used in this paper require moving one potential well while holding the second potential well stationary. To avoid cross- talk between different wells, the potential governing all trapping zones is considered when generating the waveforms.

We can insert the individual addressing and detection sequence at A_aB_b or B_aA_b in sequence (2) to encode the spin state of each ion before reordering and to detect the ion positions after reordering. The encoding is performed using a pair of co-linear Raman beams in the configurations S_aR_b and L_aS_b, addressing only the ions located at S. To verify a position swap between the two ions, we first apply a laser pulse for various durations to Rabi-flop ion a in the configuration S_aR_b. After the reordering sequence, a population oscillation as a function of pulse duration is detected only in S_aL_b (on ion a), and not in R_aS_b (on ion b) as shown in Figure 3b, indicating successful reordering. Rabi-flopping ion b in the same fashion yields a similar result, now with b exhibiting population oscillations and a remaining in the same state.

We also show that qubit coherence is maintained after reordering by applying a Ramsey sequence to each ion individually. We apply a $\pi/2$-pulse on ion a (b) in the configuration S_aR_b (L_aS_b), execute the reordering, and apply the second $\pi/2$-pulse with a variable phase relative to that of the first $\pi/2$-pulse by addressing ion a (b) in the reverse configuration S_aL_b (R_aS_b). The resulting Ramsey fringes show a contrast close to 1 for both ions addressed as shown in Figure 3c. The observed phase shift is mainly caused by the different durations that the two ions integrate over; a −1.7 kHz frequency difference between the qubits and the local oscillator corresponds to phase shifts of ≈ −18.2 rad for ion a and ≈ −28.7 rad for ion b. The frequency difference is due to the AC-Stark shift on the qubit transition from the laser beams implementing the Ramsey pulses, whose frequency difference is set to be on resonance while rotating the state of the ions in the presence of the AC-Stark shift. In addition, AC-Zeeman shifts and a magnetic field gradient across the trap are non-negligible when shuttling ions across millimeter length scales in our setup. A separate investigation shows that the AC-Zeeman shifts on the qubit transition ($|\uparrow\rangle \leftrightarrow |\downarrow\rangle$) of $^9Be^+$ vary by 10 Hz over a distance of about 15 μm along the x-direction at S. From a measured static magnetic field gradient of $\approx 4.1 \times 10^{-3}$ T m^{-1} and the second-order field sensitivity coefficient $c_2 = 3.05 \times 10^{11}$ Hz T^{-2},[34] we estimate a qubit frequency shift of ≈ 1 mHz over 15 μm.[34,41] These effects will need to be minimized, properly calibrated, or reduced by dynamical decoupling or error correction in future large-scale devices.

The axial temperature of each ion after reordering, measured through sideband thermometry, indicates that the full sequence introduces an average motional excitation of 1.1(1) for ion b and 1.7(1) for ion a (Figure 3d,e). The measured motional excitation after reordering is a factor of two to three times larger than the values obtained by summing the excitation of the constituent primitives. We believe that the additional excitation can be attributed to non-continuous concatenation and heating during idle periods

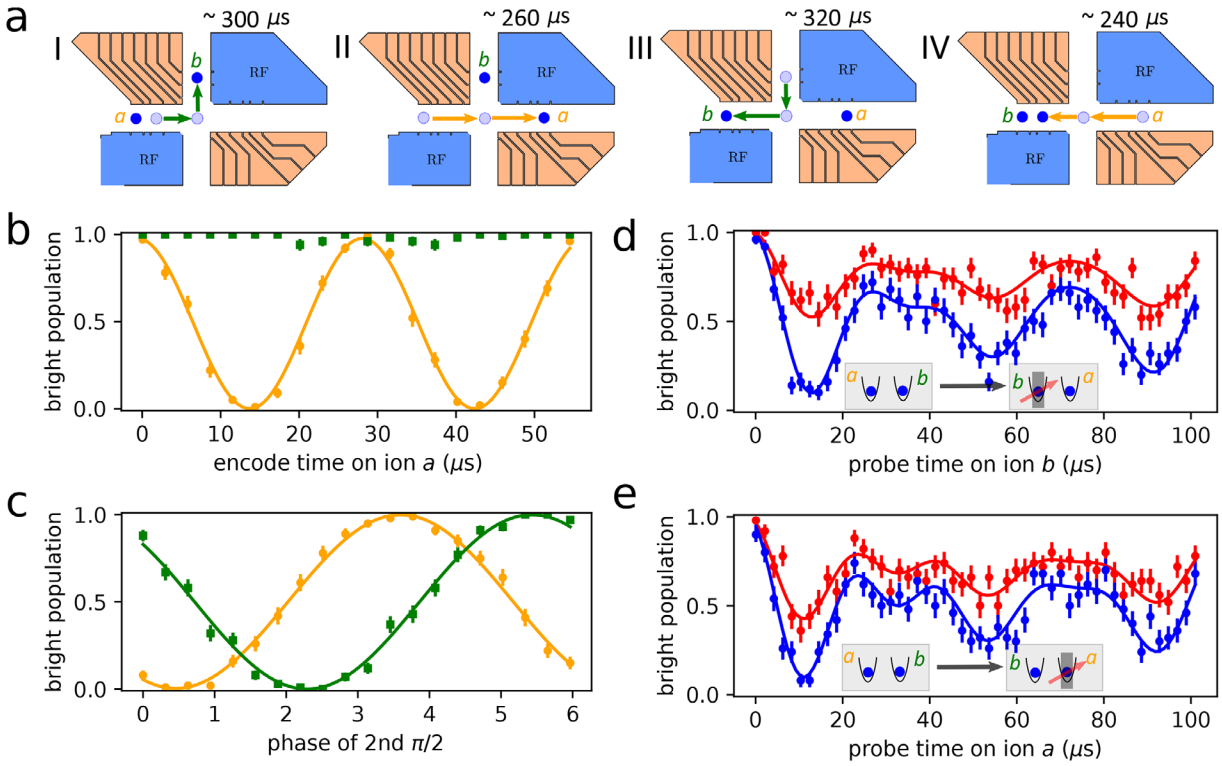

Figure 3. Reordering two $^{9}Be^{+}$ ions using the X-junction. a) Schematic representation of reordering sequence. Two ions *a* and *b* in the double well potential are shuttled sequentially through the junction to separated regions of the trap array, and then moved back to the initial well with their order swapped. The arrows (orange for ion *a* and green for ion *b*) indicate the trajectories of each ion (light blue circles) and the blue circles represent the end points of the primitives on the trajectories. b) Ion *a* is excited using a single-qubit rotation in the configuration S_aR_b, and a Rabi oscillation is observed in S_aL_b (orange) after the reordering sequence. No population oscillation is observed for detection performed in R_aS_b (green), while ion *b* is ideally in *S*. c) Coherence of the internal states of ion *a* (orange) and *b* (green) is maintained in two corresponding Ramsey sequences enclosing an exchange of ion positions and addressing one of the ions respectively. The phase shifts (0.46(2) rad for ion *a* (orange) as the offset of the fringe minimum from 0 and 2.29(2) rad for ion *b* (green)) arise mainly from the durations that the two ions accumulate phase due to a frequency shift relative to the local oscillator. See text for more details. d,e) The temperatures of the two $^{9}Be^{+}$ ions are probed on the red (red dots) and blue (blue dots) sidebands after the reordering sequence. Fits to the Rabi-oscillation model outlined in the Supporting Information (solid lines) result in average occupation numbers of 1.1(1) for ion *b* and 1.7(1) for ion *a*.

in static wells, but this requires further experimental and theoretical studies.

4. Potential Large-Scale Configurations

The physical platforms used to realize a quantum information processor determine its qubit connectivity. In general, higher connectivity increases the efficiency of implementing complex quantum algorithms. This was, for example, observed in recent studies on variational quantum simulation of electronic structures of small molecules.[42] Here, we briefly introduce several architectures for scaling quantum devices based on trapped ions and compare their expected qubit connectivity. Related discussions were published previously in refs. [43, 44].

4.1. 1D Chain of Individually Addressed Ions (Figure 4a)

All ions are trapped in a single well and are connected by the long-range Coulomb interaction, while individual control of each ion is realized by tightly focused laser beams.[45] A theoretical study determined this method to be applicable for an arbitrarily long chain of ions,[46] and experimentally, two-qubit gates between any two qubits within a 11-qubit ion chain have been performed.[47] Alternatively, individual control of ions can also be achieved by utilizing gradients of the confining trap RF field[48] or magnetic fields.[49]

4.2. 1D Trap Array (Figure 4b)

As an extension of the 1D chain in a single well, one can confine the ions within a 1D array of potential wells and apply global rotations on ions in each single well. The ions in different wells are then connected via linear shuttling and separation combined with swap gates or crystal rotations.[17] In such a 1D trap array, it takes $O(n)$ such rotations to transport an ion across n other ions using a sequence of crystal rotations. Considering the equivalence of reordering and swap operation, this will induce an overhead (longer circuit depth) on the order of $O(n)$ when rearranging a quantum circuit of n qubits with all-to-all

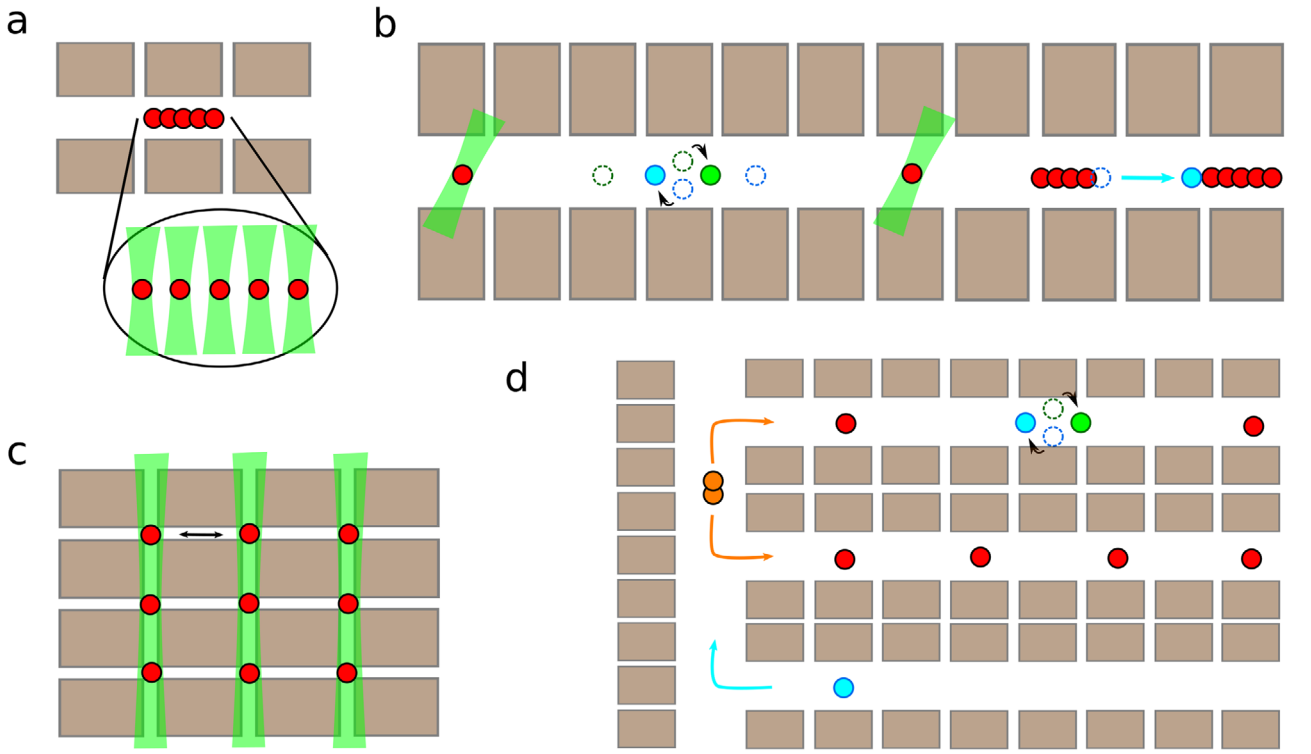

Figure 4. Chip-based multi-qubit quantum devices. a) 1D chain of individually addressed ions. Tightly focused beams allow individual addressing of ions in the chain. b) 1D trap array. Ions are confined in separated wells created by an electrode array. Separation between the wells that is large compared to the electrode dimensions allows for isolated control of each well. Coupling of a certain pair of ions is realized by repeated swap operations or crystal rotation (black arrows) and separation/recombination. c) Multi-dimensional trap lattices. Ions are confined in fixed potential wells, while the coupling between the ions is enabled by tuning the potentials (black arrow). d) Multi-dimensional trap array. Couplings between the ions are realized by shuttling information carriers (blue) or messengers (orange) through dedicated sections of the array.

connectivity to a corresponding circuit with only linear nearest-neighbor interactions.[50] By confining multiple ions in each segment, one can combine the all-to-all coupling as in Section 4.1 and the coupling between segments through shuttling. This method is predicted to achieve fault tolerance with modest reduction of the fault tolerance threshold compared to the 2D surface code despite the topological restriction posed by the 1D architecture.[51]

4.3. Multi-Dimensional Trap Lattices (Figure 4c)

Individual trapping zones are held in fixed positions in space, forming a lattice of singly occupied confining potentials with nearest-neighbor couplings tuned by bringing the traps in and out of resonance. The higher dimension provides each qubit with a larger number of nearest neighbors.[52,53] An open electrode geometry, as, for example, provided by surface electrode traps[54] is advantageous to not substantially reduce nearest-neighbor coupling by shielding from nearby electrodes. This increased connectivity between the ions therefore reduces the overhead in circuit depth for implementing a quantum circuit.[50] For example, employing a 2D square lattice where each ion has four nearest neighbors already reduces this overhead to $O(\sqrt{n})$, while 3D square lattice shares a similar feature with a reduced overhead of $O(\sqrt[3]{n})$.[50]

4.4. Multi-Dimensional Trap Array (Figure 4d)

A multi-dimensional trap array could combine all modes of operation discussed in Sections 4.1–4.3 with all-to-all connectivity between the ions by shuttling through dedicated information highways, while entangled pairs of resource ancillas can be distributed ahead of time for quantum gate teleportation to reduce the latency required by the shuttling process itself.[24] In comparison to the 1D architecture, the geometry of the trap in such an multi-dimensional architecture also reduces the average distance between any pair of ions. Small-scale reconfiguration within linear regions of the multi-dimensional array would most efficiently be done through swap gates or crystal rotations as discussed in Section 4.2, while connecting distant qubits or replacing lost ions would involve moving through junctions and dedicated transport highways. Such an architecture, more capable of reconfiguration of ion crystals, will likely be required for the construction of multiple logical qubits.[11]

5. Summary and Discussion

By combining separation and shuttling primitives, we were able to reorder two $^{9}Be^{+}$ ions using an RF junction connecting three trap zones on different sides of that junction. We verified the reordering using transport-assisted individual addressing, and

showed that quantum coherence encoded on individual qubits was maintained during the reconfiguration. We also briefly discussed example configurations for large-scale devices. In future experiments, a second ion species will enable sympathetic cooling and indirect readout of information carrying ions.[55]

Supporting Information

Supporting Information is available from the Wiley Online Library or from the author. Details on waveform generation, sideband thermometry, and mode rotation in junction are provided and refs. [56–64] are cited therein.

Acknowledgements

The thank P. Kent and J. F. Niedermeyer of NIST for helpful comments on the manuscript. This work was supported by the Office of the Director of National Intelligence (ODNI) Intelligence Advanced Research Projects Activity (IARPA), ONR, and the NIST Quantum Information Program. S.D.E. acknowledges support by the U.S. National Science Foundation under Grant No. DGE 1650115. Y.W., S.D.E., and J.J.W. are associates in the Professional Research Experience Program (PREP) operated jointly by NIST and University of Colorado Boulder.

Conflict of Interest

The authors declare no conflict of interest.

Keywords

ion reordering, ion transport, quantum information processing, trapped ions

Received: February 29, 2020
Revised: April 1, 2020
Published online: May 19, 2020

[1] S. Brewer, J.-S. Chen, A. Hankin, E. Clements, C. Chou, D. Wineland, D. Hume, D. Leibrandt, *Phys. Rev. Lett.* **2019**, *123*, 033201.
[2] T. D. Ladd, F. Jelezko, R. Laflamme, Y. Nakamura, C. Monroe, J. L. O'Brien, *Nature* **2010**, *464*, 45.
[3] L.-M. Duan, B. B. Blinov, D. L. Moehring, C. Monroe, *Quantum Inf. Comput.* **2004**, *4*, 165.
[4] C. Monroe, R. Raussendorf, A. Ruthven, K. Brown, P. Maunz, L.-M. Duan, J. Kim, *Phys. Rev. A* **2014**, *89*, 022317.
[5] D. J. Wineland, C. Monroe, W. M. Itano, D. Leibfried, B. E. King, D. M. Meekhof, *J. Res. Natl. Inst. Stand. Technol.* **1998**, *103*, 259.
[6] D. Kielpinski, C. Monroe, D. J. Wineland, *Nature* **2002**, *417*, 709.
[7] C. Ballance, T. Harty, N. Linke, M. Sepiol, D. Lucas, *Phys. Rev. Lett.* **2016**, *117*, 060504.
[8] J. Gaebler, T. Tan, Y. Lin, Y. Wan, R. Bowler, A. Keith, S. Glancy, K. Coakley, E. Knill, D. Leibfried, D. Wineland, *Phys. Rev. Lett.* **2016**, *117*, 060505.
[9] J.-S. Chen, S. Brewer, C. Chou, D. Wineland, D. Leibrandt, D. Hume, *Phys. Rev. Lett.* **2017**, *118*, 053002.
[10] S. Crain, C. Cahall, G. Vrijsen, E. E. Wollman, M. D. Shaw, V. B. Verma, S. W. Nam, J. Kim, *Commun. Phys.* **2019**, *2*, 1.
[11] A. Bermudez, X. Xu, R. Nigmatullin, J. O'Gorman, V. Negnevitsky, P. Schindler, T. Monz, U. Poschinger, C. Hempel, J. Home, F. Schmidt-Kaler, M. Biercuk, R. Blatt, S. Benjamin, M. Müller, *Phys. Rev. X* **2017**, *7*, 041061.
[12] R. B. Blakestad, C. Ospelkaus, A. P. VanDevender, J. M. Amini, J. Britton, D. Leibfried, D. J. Wineland, *Phys. Rev. Lett.* **2009**, *102*, 153002.
[13] R. B. Blakestad, C. Ospelkaus, A. P. VanDevender, J. H. Wesenberg, M. J. Biercuk, D. Leibfried, D. J. Wineland, *Phys. Rev. A* **2011**, *84*, 032314.
[14] R. Bowler, J. Gaebler, Y. Lin, T. R. Tan, D. Hanneke, J. D. Jost, J. P. Home, D. Leibfried, D. J. Wineland, *Phys. Rev. Lett.* **2012**, *109*, 080502.
[15] A. Walther, F. Ziesel, T. Ruster, S. T. Dawkins, K. Ott, M. Hettrich, K. Singer, F. Schmidt-Kaler, U. Poschinger, *Phys. Rev. Lett.* **2012**, *109*, 080501.
[16] F. Splatt, M. Harlander, M. Brownnutt, F. Zähringer, R. Blatt, W. Hänsel, *New J. Phys.* **2009**, *11*, 103008.
[17] H. Kaufmann, T. Ruster, C. T. Schmiegelow, M. A. Luda, V. Kaushal, J. Schulz, D. von Lindenfels, F. Schmidt-Kaler, U. G. Poschinger, *Phys. Rev. A* **2017**, *95*, 052319.
[18] M. W. van Mourik, E. A. Martinez, L. Gerster, P. Hrmo, T. Monz, P. Schindler, R. Blatt, arXiv:2001.02440, **2020**.
[19] D. Leibfried, E. Knill, C. Ospelkaus, D. J. Wineland, *Phys. Rev. A* **2007**, *76*, 032324.
[20] L. E. de Clercq, H. Y. Lo, M. Marinelli, D. Nadlinger, R. Oswald, V. Negnevitsky, D. Kienzler, B. Keitch, J. P. Home, *Phys. Rev. Lett.* **2016**, *116*, 080502.
[21] H. Kaufmann, T. Ruster, C. Schmiegelow, M. Luda, V. Kaushal, J. Schulz, D. von Lindenfels, F. Schmidt-Kaler, U. Poschinger, *Phys. Rev. Lett.* **2017**, *119*, 150503.
[22] T. Ruster, H. Kaufmann, M. Luda, V. Kaushal, C. Schmiegelow, F. Schmidt-Kaler, U. Poschinger, *Phys. Rev. X* **2017**, *7*, 031050.
[23] T. Tan, Y. Wan, S. Erickson, P. Bierhorst, D. Kienzler, S. Glancy, E. Knill, D. Leibfried, D. Wineland, *Phys. Rev. Lett.* **2017**, *118*, 130403.
[24] Y. Wan, D. Kienzler, S. D. Erickson, K. H. Mayer, T. R. Tan, J. J. Wu, H. M. Vasconcelos, S. Glancy, E. Knill, D. J. Wineland, A. C. Wilson, D. Leibfried, *Science* **2019**, *364*, 875.
[25] W. K. Hensinger, S. Olmschenk, D. Stick, D. Hucul, M. Yeo, M. Acton, L. Deslauriers, C. Monroe, J. Rabchuk, *Appl. Phys. Lett.* **2006**, *88*, 034101.
[26] K. Wright, J. M. Amini, D. L. Faircloth, C. Volin, S. C. Doret, H. Hayden, C. S. Pai, D. W. Landgren, D. Denison, T. Killian, R. E. Slusher, A. W. Harter, *New J. Phys.* **2013**, *15*, 033004.
[27] J. M. Amini, H. Uys, J. H. Wesenberg, S. Seidelin, J. Britton, J. J. Bollinger, D. Leibfried, C. Ospelkaus, A. P. VanDevender, D. J. Wineland, *New J. Phys.* **2010**, *12*, 033031.
[28] G. Shu, G. Vittorini, A. Buikema, C. S. Nichols, C. Volin, D. Stick, K. R. Brown, *Phys. Rev. A* **2014**, *89*, 062308.
[29] D. L. Moehring, C. Highstrete, D. Stick, K. M. Fortier, R. Haltli, C. Tigges, M. G. Blain, *New J. Phys.* **2011**, *13*, 075018.
[30] N. M. Linke, D. Maslov, M. Roetteler, S. Debnath, C. Figgatt, K. A. Landsman, K. Wright, C. Monroe, *Proc. Natl. Acad. Sci. USA* **2017**, *114*, 3305.
[31] V. Kaushal, B. Lekitsch, A. Stahl, J. Hilder, D. Pijn, C. Schmiegelow, A. Bermudez, M. Müller, F. Schmidt-Kaler, U. Poschinger, *AVS Quantum Sci.* **2020**, *2*, 014101.
[32] R. B. Blakestad, *Ph.D. Thesis*, University of Colorado **2010**.
[33] D. J. Berkeland, J. D. Miller, J. C. Bergquist, W. M. Itano, D. J. Wineland, *J. Appl. Phys.* **1998**, *83*, 5025.
[34] C. Langer, R. Ozeri, J. D. Jost, J. Chiaverini, B. DeMarco, A. Ben-Kish, R. B. Blakestad, J. Britton, D. B. Hume, W. M. Itano, D. Leibfried, R. Reichle, T. Rosenband, T. Schaetz, P. O. Schmidt, D. J. Wineland, *Phys. Rev. Lett.* **2005**, *95*, 060502.
[35] W. Nagourney, J. Sandberg, H. Dehmelt, *Phys. Rev. Lett.* **1986**, *56*, 2797.
[36] T. Sauter, W. Neuhauser, R. Blatt, P. Toschek, *Phys. Rev. Lett.* **1986**, *57*, 1696.

[37] J. C. Bergquist, R. G. Hulet, W. M. Itano, D. J. Wineland, *Phys. Rev. Lett.* **1986**, *57*, 1699.
[38] D. M. Meekhof, C. Monroe, B. E. King, W. M. Itano, D. J. Wineland, *Phys. Rev. Lett.* **1996**, *76*, 1796.
[39] D. M. Meekhof, C. Monroe, B. E. King, W. M. Itano, D. J. Wineland, *Phys. Rev. Lett.* **1996**, *77*, 2346.
[40] J. P. Home, A. M. Steane, *Quantum Inf. Comput.* **2006**, *6*, 289.
[41] C. E. Langer, *Ph.D. Thesis*, University of Colorado **2006**.
[42] A. Kandala, A. Mezzacapo, K. Temme, M. Takita, M. Brink, J. M. Chow, J. M. Gambetta, *Nature* **2017**, *549*, 242.
[43] A. K. Ratcliffe, R. L. Taylor, J. J. Hope, A. R. Carvalho, *Phys. Rev. Lett.* **2018**, *120*, 220501.
[44] J. Welzel, A. Bautista-Salvador, C. Abarbanel, V. Wineman-Fisher, C. Wunderlich, R. Folman, F. Schmidt-Kaler, *Eur. Phys. J. D* **2011**, *65*, 285.
[45] H. C. Nägerl, D. Leibfried, H. Rohde, G. Thalhammer, J. Eschner, F. Schmidt-Kaler, R. Blatt, *Phys. Rev. A* **1999**, *60*, 145.
[46] K. A. Landsman, Y. Wu, P. H. Leung, D. Zhu, N. M. Linke, K. R. Brown, L. Duan, C. Monroe, *Phys. Rev. A* **2019**, *100*, 022332.
[47] K. Wright, K. Beck, S. Debnath, J. Amini, Y. Nam, N. Grzesiak, J.-S. Chen, N. Pisenti, M. Chmielewski, C. Collins, K. M. Hudek, J. Mizrahi, J. D. Wong-Campos, S. Allen, J. Apisdorf, P. Solomon, M. Williams, A. M. Ducore, A. Blinov, S. M. Kreikemeier, V. Chaplin, M. Keesan, C. Monroe, J. Kim, arXiv:1903.08181, **2019**.
[48] D. Leibfried, *Phys. Rev. A* **1999**, *60*, R3335.
[49] C. Piltz, T. Sriarunothai, A. F. Varón, C. Wunderlich, *Nat. Commun.* **2014**, *5*, 4679.
[50] D. Cheung, D. Maslov, S. Severini, presented at Proc. Workshop on Quantum Information, Palermo, Italy, June **2007**.
[51] Y. Li, S. C. Benjamin, *npj Quantum Inf.* **2018**, *4*, 25.
[52] R. Schmied, J. Wesenberg, D. Leibfried, *Phys. Rev. Lett.* **2009**, *102*, 233002.
[53] F. N. Krauth, J. Alonso, J. P. Home, *J. Phys. B* **2014**, *48*, 015001.
[54] J. Chiaverini, R. B. Blakestad, J. Britton, J. D. Jost, C. Langer, D. Leibfried, R. Ozeri, D. J. Wineland, *Quantum Inf. Comput.* **2005**, *5*, 419.
[55] T. R. Tan, J. P. Gaebler, Y. Lin, Y. Wan, R. Bowler, D. Leibfried, D. J. Wineland, *Nature* **2015**, *528*, 380.
[56] See bem package at https://github.com/nist-ionstorage/bem
[57] See electrode package at https://github.com/nist-ionstorage/electrode.
[58] See cvxopt package at https://cvxopt.org.
[59] D. F. V. James, *Appl. Phys. B* **1998**, *66*, 181.
[60] R. Bowler, U. Warring, J. W. Britton, B. C. Sawyer, J. Amini, *Rev. Sci. Instrum.* **2013**, *84*, 033108.
[61] R. Bowler, *Ph.D. Thesis*, University of Colorado **2015**.
[62] Y. Wan, F. Gebert, F. Wolf, P. O. Schmidt, *Phys. Rev. A* **2015**, *91*, 043425.
[63] K. Fujii, K. Higashida, R. Kato, Y. Wada, *Yokohama Mathematical Journal* **2006**, *53*, 63.
[64] H. Kaufmann, *Ph.D. Thesis*, Johannes Gutenberg-Universität, Mainz **2017**.